LETTER

doi:10.1038/nature25149

An extreme magneto-ionic environment associated with the fast radio burst source FRB 121102

D. Michilli[1,2]*, A. Seymour[3]*, J. W. T. Hessels[1,2]*, L. G. Spitler[4], V. Gajjar[5,6,7], A. M. Archibald[1,2], G. C. Bower[8], S. Chatterjee[9], J. M. Cordes[9], K. Gourdji[2], G. H. Heald[10], V. M. Kaspi[11], C. J. Law[12], C. Sobey[10,13], E. A. K. Adams[1,14], C. G. Bassa[1], S. Bogdanov[15], C. Brinkman[16], P. Demorest[17], F. Fernandez[3], G. Hellbourg[12], T. J. W. Lazio[18], R. S. Lynch[19,20], N. Maddox[1], B. Marcote[21], M. A. McLaughlin[20,22], Z. Paragi[21], S. M. Ransom[23], P. Scholz[24], A. P. V. Siemion[12,25,26], S. P. Tendulkar[11], P. Van Rooy[27], R. S. Wharton[4] & D. Whitlow[3]

Fast radio bursts are millisecond-duration, extragalactic radio flashes of unknown physical origin[1–3]. The only known repeating fast radio burst source[4–6]—FRB 121102—has been localized to a star-forming region in a dwarf galaxy[7–9] at redshift 0.193 and is spatially coincident with a compact, persistent radio source[7,10]. The origin of the bursts, the nature of the persistent source and the properties of the local environment are still unclear. Here we report observations of FRB 121102 that show almost 100 per cent linearly polarized emission at a very high and variable Faraday rotation measure in the source frame (varying from $+1.46 \times 10^5$ radians per square metre to $+1.33 \times 10^5$ radians per square metre at epochs separated by seven months) and narrow (below 30 microseconds) temporal structure. The large and variable rotation measure demonstrates that FRB 121102 is in an extreme and dynamic magneto-ionic environment, and the short durations of the bursts suggest a neutron star origin. Such large rotation measures have hitherto been observed[11,12] only in the vicinities of massive black holes (larger than about 10,000 solar masses). Indeed, the properties of the persistent radio source are compatible with those of a low-luminosity, accreting massive black hole[10]. The bursts may therefore come from a neutron star in such an environment or could be explained by other models, such as a highly magnetized wind nebula[13] or supernova remnant[14] surrounding a young neutron star.

Using the 305-m William E. Gordon Telescope at the Arecibo Observatory, we detected 16 bursts from FRB 121102 at radio frequencies in the range 4.1–4.9 GHz (Table 1). Complete polarization parameters were recorded at a 10.24-μs time resolution. See Methods and Extended Data Figs 1–6 for observation and analysis details.

The 4.5-GHz bursts have typical widths smaller than about 1 ms, which are narrower than the 2–9-ms bursts previously detected at lower frequencies[5,15]. In some cases they show multiple components and structures close to the sampling time of the data. Burst 6 (Table 1) is particularly striking, with a width smaller than about 30 μs (which constrains the size of the emitting region to below about 10 km, assuming no other geometric or relativistic effects). The evolution of burst morphology with frequency complicates the determination[5] of the dispersion measure ($\mathrm{DM} = \int_0^d n_\mathrm{e}(l)\mathrm{d}l$, where d is the distance to the source in parsec, l is the line-of-sight position and n_e is the electron density in electrons per cubic centimetre), but aligning the narrow component in burst 6 results in $\mathrm{DM} = 559.7 \pm 0.1\ \mathrm{pc\ cm^{-3}}$, which is consistent[4,5,15,16] with other bursts detected since 2012 and suggests that any real dispersion measure variations are below the level of about 1%.

After correcting for Faraday rotation and accounting for about 2% depolarization from the finite channel widths, the bursts are consistently linearly polarized to about 100% (Fig. 1). The polarization angles $\mathrm{PA} = \mathrm{PA}_\infty + \theta$ (where PA_∞ is a reference angle at infinite frequency, $\theta = \mathrm{RM}\lambda^2$ is the rotation angle of the electric field vector, RM is the Faraday rotation measure and λ is the observing wavelength) are flat across the observed frequency range and burst envelopes (ΔPA smaller than about $5°\ \mathrm{ms^{-1}}$). This could mean that the burst durations reflect the timescale of the emission process and not the rate of a rotating beam sweeping across the line of sight. Any circular polarization is lower than a few per cent of the total intensity. The Faraday rotation measure is defined as $\mathrm{RM} = 0.81 \int_d^0 B_\parallel(l) n_\mathrm{e}(l)\mathrm{d}l$, where $B_\parallel$ is the line-of-sight magnetic field strength (in microgauss); by convention, the rotation measure is positive when the magnetic field points towards the observer. On average, the observed rotation measure is $\mathrm{RM_{obs}} = (+1.027 \pm 0.001) \times 10^5\ \mathrm{rad\ m^{-2}}$ and varies by about 0.5% between Arecibo observing sessions spanning a month (Fig. 2; Table 1). The lack of polarization in previous burst detections[15,16] at 1.1–2.4 GHz is consistent with the relatively coarse frequency channels that cause bandwidth depolarization and constrains $|\mathrm{RM_{obs}}|$ to above about $10^4\ \mathrm{rad\ m^{-2}}$ at those epochs.

Confirmation of this extreme Faraday rotation comes from independent observations at 4–8 GHz with the 110-m Robert C. Byrd Green Bank Telescope (GBT), which give $\mathrm{RM_{obs}} = (+0.935 \pm 0.001) \times 10^5\ \mathrm{rad\ m^{-2}}$ at an epoch seven months after the Arecibo detections. The GBT and Arecibo $\mathrm{RM_{obs}}$ values differ with high

[1]ASTRON, Netherlands Institute for Radio Astronomy, Postbus 2, 7990 AA Dwingeloo, The Netherlands. [2]Anton Pannekoek Institute for Astronomy, University of Amsterdam, Science Park 904, 1098 XH Amsterdam, The Netherlands. [3]National Astronomy and Ionosphere Center, Arecibo Observatory, Puerto Rico 00612, USA. [4]Max-Planck-Institut für Radioastronomie, Auf dem Hügel 69, D-53121 Bonn, Germany. [5]Space Science Laboratory, 7 Gauss Way, University of California, Berkeley, California 94710, USA. [6]Xinjiang Astronomical Observatory, CAS, 150 Science 1-Street, Urumqi, Xinjiang 830011, China. [7]Key Laboratory of Radio Astronomy, Chinese Academy of Sciences, Nanjing 210008, China. [8]Academia Sinica Institute of Astronomy and Astrophysics, 645 N. A'ohoku Place, Hilo, Hawaii 96720, USA. [9]Cornell Center for Astrophysics and Planetary Science and Department of Astronomy, Cornell University, Ithaca, New York 14853, USA. [10]CSIRO Astronomy and Space Science, 26 Dick Perry Avenue, Kensington, Western Australia 6151, Australia. [11]Department of Physics and McGill Space Institute, McGill University, 3600 University, Montréal, Quebec H3A 2T8, Canada. [12]Department of Astronomy and Radio Astronomy Lab, University of California, Berkeley, California 94720, USA. [13]International Centre for Radio Astronomy Research - Curtin University, GPO Box U1987, Perth, Western Australia 6845, Australia. [14]Kapteyn Astronomical Institute, University of Groningen, Postbus 800, 9700 AA Groningen, The Netherlands. [15]Columbia Astrophysics Laboratory, Columbia University, New York, New York 10027, USA. [16]Physics Department, University of Vermont, Burlington, Vermont 05401, USA. [17]National Radio Astronomy Observatory, PO Box O, Socorro, New Mexico 87801 USA. [18]Jet Propulsion Laboratory, California Institute of Technology, Pasadena, California 91109, USA. [19]Green Bank Observatory, PO Box 2, Green Bank, West Virginia 24944, USA. [20]Center for Gravitational Waves and Cosmology, Chestnut Ridge Research Building, Morgantown, West Virginia 26505, USA. [21]Joint Institute for VLBI ERIC, Postbus 2, 7990 AA Dwingeloo, The Netherlands. [22]Department of Physics and Astronomy, West Virginia University, Morgantown, West Virginia 26506, USA. [23]National Radio Astronomy Observatory, Charlottesville, Virginia 22903, USA. [24]National Research Council of Canada, Herzberg Astronomy and Astrophysics, Dominion Radio Astrophysical Observatory, PO Box 248, Penticton, British Columbia V2A 6J9, Canada. [25]Radboud University, Nijmegen, Comeniuslaan 4, 6525 HP Nijmegen, The Netherlands. [26]SETI Institute, 189 North Bernardo Avenue 200, Mountain View, California 94043, USA. [27]Department of Electrical Engineering and Computer Science, Case Western Reserve University, Cleveland, Ohio 44106, USA.
*These authors contributed equally to this work.

Table 1 | Properties of Arecibo (1–16) and GBT (GBT-1 and GBT-2) bursts

Burst	Modified Julian date	Width (ms)	S (Jy)	F (Jy ms)	RM_{obs} (rad m^{-2})	PA_∞ (°)	RM_{global} (rad m^{-2})	PA_∞^{global} (°)
1	57,747.1295649013	0.80	0.9	0.7	+102,741±9	49±2		
2	57,747.1371866766	0.85	0.3	0.2	+102,732±34	55±9		
3	57,747.1462710273	0.22	0.8	0.2	+102,689±18	64±5		
4	57,747.1515739398	0.55	0.2	0.09	–	–		
5	57,747.1544674919	0.76	0.2	0.1	–	–	+102,708±4	
6	57,747.1602892954	0.03	1.8	0.05	+102,739±35	49±9		
7	57,747.1603436945	0.31	0.6	0.2	+102,663±33	71±9		
8	57,747.1658277033	1.36	0.4	0.5	+102,668±18	67±4		
9	57,747.1663749941	1.92	0.2	0.3	–	–		58±1
10	57,747.1759674338	0.98	0.2	0.2	–	–		
11	57,748.1256436428	0.95	0.1	0.1	–	–		
12	57,748.1535244366	0.42	0.4	0.2	+102,508±35	63±10		
13	57,748.1552149312	0.78	0.8	0.6	+102,522±17	59±4	+102,521±4	
14	57,748.1576076618	0.15	1.2	0.2	+102,489±18	67±5		
15	57,748.1756968287	0.54	0.4	0.4	+102,492±37	64±10		
16	57,772.1290302972	0.74	0.8	0.6	+103,020±12	64±3	+103,039±4	
GBT-1	57,991.5801286366	0.59	0.4	0.2	+93,526±72	73±8		
GBT-2	57,991.5833032369	0.27	0.9	0.2	+93,533±42	71±4	+93,573±24	68±2

Modified Julian dates are referenced to infinite frequency at the Solar System barycentre; their uncertainties are of the order of the burst widths. Widths have uncertainties of about 10 μs. Peak flux densities S and fluences F have about 20% fractional uncertainties. Rotation measures are not corrected for redshift, and polarization angles are referenced to infinite frequency. Bursts with no individual rotation measure entry (–) were too weak to reliably fit on their own. The last two columns refer to a global fit of all bursts. All errors are 1σ; see Methods for observational details.

statistical significance and indicate that the rotation measure can vary by at least 10% on half-year timescales (Table 1 and Extended Data Fig. 5).

The Faraday rotation must come almost exclusively from within the host galaxy; the expected Milky Way contribution[17] is -25 ± 80 rad m^{-2}, while estimated intergalactic medium contributions[18] are lower than about 10^2 rad m^{-2}. In the source reference frame, $RM_{src} = RM_{obs}(1+z)^2 = +1.46 \times 10^5$ rad m^{-2} and $+1.33 \times 10^5$ rad m^{-2} for the Arecibo and GBT data, respectively, where z is the redshift. Without a correspondingly large change in the dispersion measure, the observed variations in rotation measure indicate that the Faraday rotation comes from a compact region with a high magnetic field. Furthermore, that region must be close to FRB 121102 because it is very unlikely that an unrelated small structure with the required high magnetic field is coincidentally in the line of sight.

We can fit all 16 Arecibo bursts with a single polarization angle $PA_\infty^{global} = 58° \pm 1°$ (referenced to infinite frequency; measured anticlockwise from North to East) and a single RM_{global} per observation day (Table 1). However, we cannot rule out small changes in the

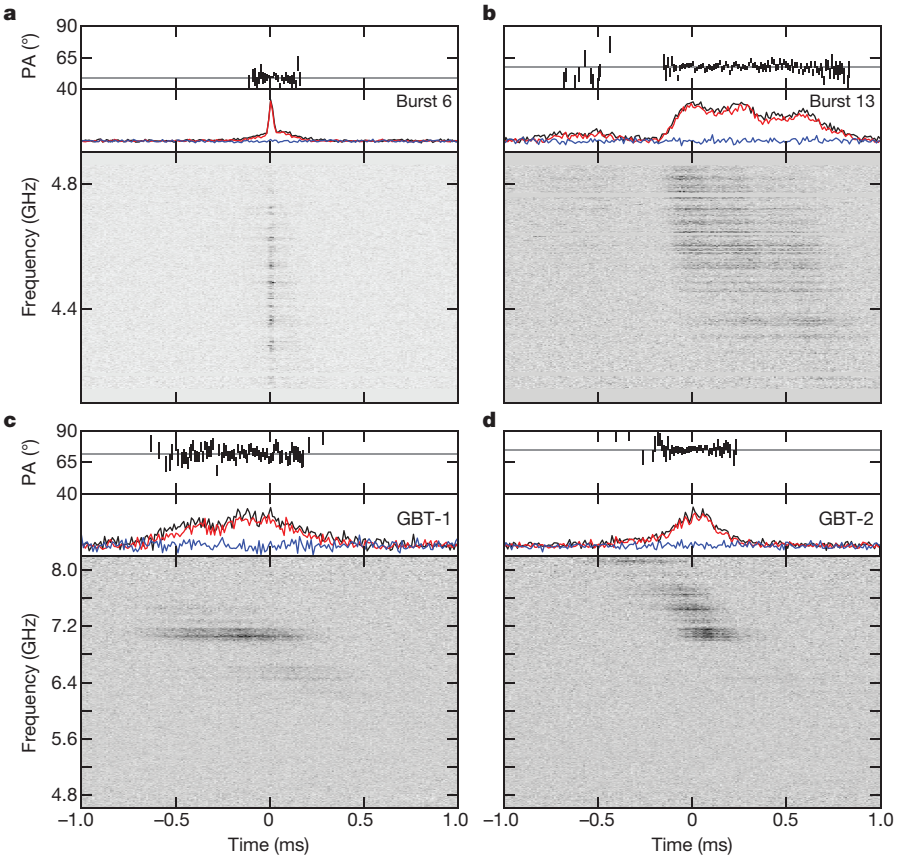

Figure 1 | Polarization angles, pulse profile and spectrum of four bursts. The grey horizontal lines indicate the average polarization angle of each burst. The red and blue lines indicate linear and circular polarization profiles, respectively, while the black line is the total intensity. **a**, **b**, The Arecibo bursts are plotted with time and frequency resolutions of 10.24 μs and 1.56 MHz, respectively. **c**, **d**, The GBT bursts are plotted with time and frequency resolutions of 10.24 μs and 5.86 MHz, respectively.

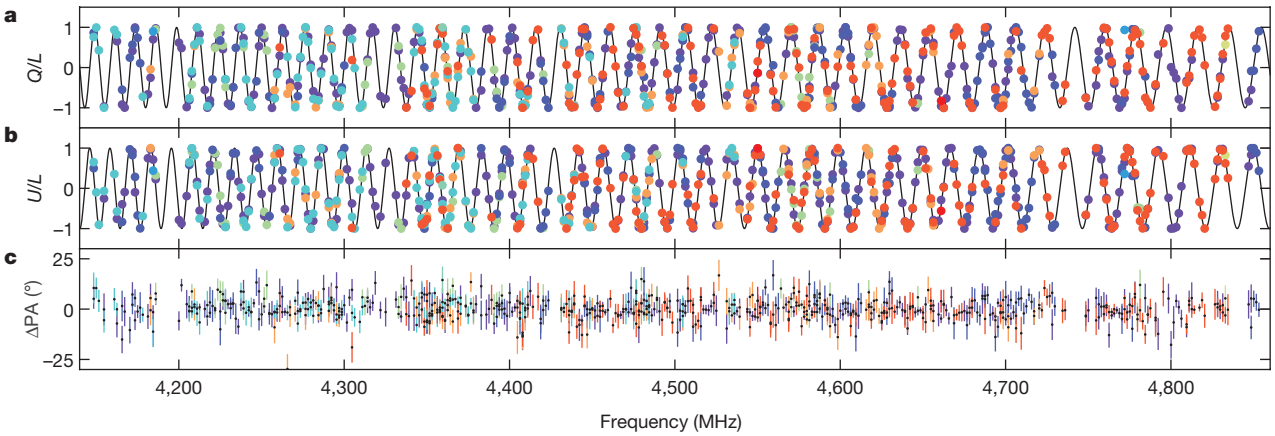

Figure 2 | Faraday rotation in the bursts. a, **b**, Variations of the Stokes parameters Q (**a**) and U (**b**) with frequency, normalized by the total linear polarization ($L=\sqrt{Q^2+U^2}$), for the six brightest Arecibo bursts detected on modified Julian date 57,747. Different bursts are plotted using different colours. Only data points with signal-to-noise ratio higher than 5 are plotted and do not include uncertainties. The black lines represent the best-fitting Faraday rotation model for the global values reported in Table 1. **c**, Difference between calculated and measured polarization angles (ΔPA) with 1σ uncertainties around the central values, which are indicated with black dots.

rotation measure (below about 50 rad m^{-2}) and polarization angle (lower than approximately 10°) between bursts. The GBT data are not well modelled by the use of a single $\mathrm{PA}_{\infty}^{\mathrm{global}}$ value, but this could be an instrumental difference or reflection of the higher observing frequency. The near constancy of the polarization angle suggests that the burst emitter has a stable geometric orientation with respect to the observer. A linear polarization fraction higher than about 98% at a single rotation measure constrains turbulent scatter[19] as $\sigma_{\mathrm{RM}}<25$ rad m^{-2} and the linear gradient across the source as $\Delta_{\mathrm{RM}}<20$ rad m^{-2}, and there is no evidence of deviations from the squared-wavelength (λ^2) scaling of the Faraday rotation effect. Analysis with the RM Synthesis technique and the deconvolution procedure RMCLEAN also implies a 'Faraday-thin' medium (see Methods).

In the rest frame, the host galaxy contributes a dispersion measure $\mathrm{DM_{host}}\approx 70$–$270$ pc cm^{-3} to the total dispersion measure of the bursts[8]. Given $\mathrm{RM_{src}}$, this corresponds to an estimated line-of-sight magnetic field $B_{\parallel}=0.6f_{\mathrm{DM}}$–$2.4f_{\mathrm{DM}}$ mG. This is a lower-limit range because the dispersion measure contribution that is related to the observed rotation measure ($\mathrm{DM_{RM}}$) could be much smaller than the total dispersion measure contribution of the host ($\mathrm{DM_{host}}$, dominated by the star-forming region), which we quantify by the scaling factor $f_{\mathrm{DM}}=\mathrm{DM_{host}}/\mathrm{DM_{RM}}\geq 1$. For comparison, typical magnetic field strengths within the interstellar medium of our Galaxy[20] are only about 5 μG.

We can constrain the electron density, electron temperature (T_{e}) and length scale (L_{RM}) of the region causing the Faraday rotation by balancing the magnetic field and thermal energy densities (Extended Data Fig. 6). For example, assuming equipartition and $T_{\mathrm{e}}=10^6$ K, we find a density of $n_{\mathrm{e}}\approx 10^2$ cm^{-3} on a length scale of $L_{\mathrm{RM}}\approx 1$ pc, comparable to the upper limit of the size of the persistent source[10].

A star-forming region, such as that hosting FRB 121102, will contain H II regions of ionized hydrogen. Although very compact H II regions have sufficiently high magnetic fields and electron densities to explain the large rotation measure, the constraints from $\mathrm{DM_{host}}$ and the absence of free–free absorption of the bursts exclude a wide range of H II region sizes and densities[21] for typical temperatures of 10^4 K.

The environment around a massive black hole is consistent with the n_{e}, L_{RM} and T_{e} constraints[22], and the properties of the persistent source are compatible with those of a low-luminosity, accreting massive black hole[10]. The high rotation measure towards the Galactic Centre magnetar[23] PSR J1745−2900 (Fig. 3), $\mathrm{RM}=-7\times 10^4$ rad m^{-2}, provides an intriguing observational analogy for a scenario in which the bursts are produced by a neutron star in the immediate environment of a massive black hole. However, the bursts of FRB 121102 are many orders of magnitude more energetic than those of PSR J1745−2900 or any Galactic pulsar.

An alternative description of FRB 121102 has been proposed by a millisecond magnetar model[8,10,13]. According to that model, one would expect a surrounding supernova remnant and nebula powered by the central neutron star. The n_{e}, L_{RM} and T_{e} constraints are broadly compatible with the conditions in pulsar-wind nebulae, but dense filaments like those seen in the Crab Nebula[24] may need to be invoked to explain the high and variable rotation measure of FRB 121102. In a young neutron star scenario, an expanding supernova remnant could also in principle produce a high rotation measure by sweeping up surrounding ambient medium and progenitor ejecta[25]. A more detailed discussion of these scenarios is provided in Methods, and more exotic models also remain possible[26].

Regardless of its nature, FRB 121102 clearly inhabits an extreme magneto-ionic environment. In contrast, Galactic pulsars with comparable dispersion measures have rotation measures that are

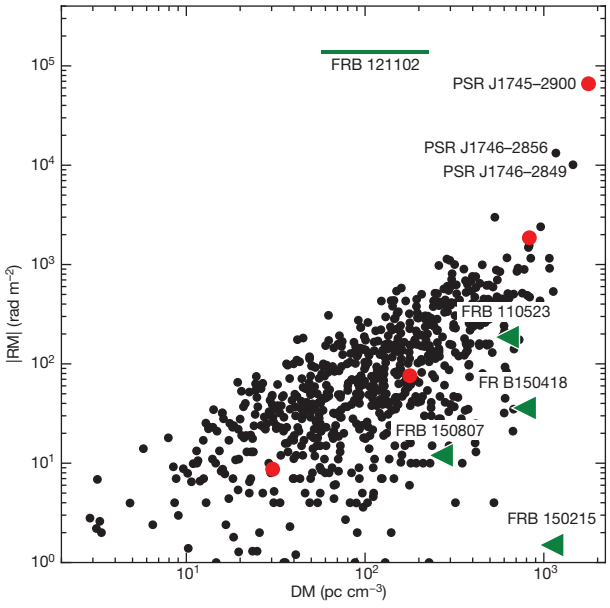

Figure 3 | Magnitude of rotation measure versus dispersion measure for fast radio bursts and Galactic pulsars. Radio-loud magnetars are highlighted with red dots, while radio pulsars and magnetars closest to the Galactic Centre[30] are labelled by name. The green bar represents FRB 121102 and the uncertainty on the dispersion measure contribution of the host galaxy[8]. Green triangles are other fast radio bursts with measured rotation measure; here the dispersion measure is the upper limit of the contribution from the host galaxy.

smaller than a hundredth of the RM_{src} value of FRB 121102 (Fig. 3), which is also about 500 times larger than those previously detected in fast radio bursts[27]. The five other known fast radio bursts with polarimetric measurements present a heterogeneous picture, with a range of polarization fractions and rotation measures[3]. As previously considered[28], the large Faraday rotation of FRB 121102 further suggests that fast radio bursts with no detectable linear polarization may actually have very large $|RM|$, higher than 10^4–10^5 rad m^{-2}, that was undetectable because of the limited frequency resolution (0.4-MHz channels at 1.4 GHz) of the observations.

Monitoring the rotation measure and polarization angle of FRB 121102 with time, along with searches for polarization and Faraday rotation from the persistent source, can help differentiate among competing models. FRB 121102 is unusual not only because of its large rotation measure but also because it is the only known repeating fast radio burst. This may indicate that FRB 121102 is a fundamentally different type of source compared to the rest of the fast radio burst population; future measurements may investigate a possible correlation between fast radio burst repetition and rotation measure. Perhaps the markedly higher activity level of FRB 121102 compared to other known fast radio bursts is predominantly a consequence of its environment; for example, because these magnetized structures can also boost the detectability of the bursts via plasma lensing[29].

Online Content Methods, along with any additional Extended Data display items and Source Data, are available in the online version of the paper; references unique to these sections appear only in the online paper.

Received 1 November; accepted 20 November 2017.

1. Lorimer, D. R., Bailes, M., McLaughlin, M. A., Narkevic, D. J. & Crawford, F. A bright millisecond radio burst of extragalactic origin. *Science* **318,** 777–780 (2007).
2. Thornton, D. *et al.* A population of fast radio bursts at cosmological distances. *Science* **341,** 53–56 (2013).
3. Petroff, E. *et al.* FRBCAT: the fast radio burst catalogue. *Publ. Astron. Soc. Aust.* **33,** e045 (2016).
4. Spitler, L. G. *et al.* Fast radio burst discovered in the Arecibo pulsar ALFA survey. *Astrophys. J.* **790,** 101 (2014).
5. Spitler, L. G. *et al.* A repeating fast radio burst. *Nature* **531,** 202–205 (2016).
6. Petroff, E. *et al.* A survey of FRB fields: limits on repeatability. *Mon. Not. R. Astron. Soc.* **454,** 457–462 (2015).
7. Chatterjee, S. *et al.* A direct localization of a fast radio burst and its host. *Nature* **541,** 58–61 (2017).
8. Tendulkar, S. P. *et al.* The host galaxy and redshift of the repeating fast radio burst FRB 121102. *Astrophys. J.* **834,** L7 (2017).
9. Bassa, C. G. *et al.* FRB 121102 is coincident with a star-forming region in its host galaxy. *Astrophys. J.* **843,** L8 (2017).
10. Marcote, B. *et al.* The repeating fast radio burst FRB 121102 as seen on milliarcsecond angular scales. *Astrophys. J.* **834,** L8 (2017).
11. Bower, G. C., Wright, M. C. H., Falcke, H. & Backer, D. C. Interferometric detection of linear polarization from Sagittarius A* at 230 GHz. *Astrophys. J.* **588,** 331–337 (2003).
12. Marrone, D. P., Moran, J. M., Zhao, J.-H. & Rao, R. An unambiguous detection of Faraday rotation in Sagittarius A*. *Astrophys. J.* **654,** L57–L60 (2007).
13. Metzger, B. D., Berger, E. & Margalit, B. Millisecond magnetar birth connects frb 121102 to superluminous supernovae and long-duration gamma-ray bursts. *Astrophys. J.* **841,** 14 (2017).
14. Piro, A. L. The impact of a supernova remnant on fast radio bursts. *Astrophys. J.* **824,** L32 (2016).
15. Scholz, P. *et al.* The repeating fast radio burst FRB 121102: multi-wavelength observations and additional bursts. *Astrophys. J.* **833,** 177 (2016).
16. Scholz, P. *et al.* Simultaneous X-ray, gamma-ray, and radio observations of the repeating fast radio burst FRB 121102. *Astrophys. J.* **846,** 80 (2017).
17. Oppermann, N. *et al.* Estimating extragalactic Faraday rotation. *Astron. Astrophys.* **575,** A118 (2015).
18. Akahori, T., Ryu, D. & Gaensler, B. M. Fast radio bursts as probes of magnetic fields in the intergalactic medium. *Astrophys. J.* **824,** 105 (2016).
19. O'Sullivan, S. P. *et al.* Complex Faraday depth structure of active galactic nuclei as revealed by broad-band radio polarimetry. *Mon. Not. R. Astron. Soc.* **421,** 3300–3315 (2012).
20. Haverkorn, M. in *Magnetic Fields in Diffuse Media* (eds Lazarian, A. *et al.*) 483–506 (Springer, 2015).
21. Hunt, L. K. & Hirashita, H. The size-density relation of extragalactic H II regions. *Astron. Astrophys.* **507,** 1327–1343 (2009).
22. Quataert, E., Narayan, R. & Reid, M. J. What is the accretion rate in Sagittarius A*? *Astrophys. J.* **517,** L101–L104 (1999).
23. Eatough, R. P. *et al.* A strong magnetic field around the supermassive black hole at the centre of the Galaxy. *Nature* **501,** 391–394 (2013).
24. Davidson, K. & Fesen, R. A. Recent developments concerning the Crab Nebula. *Annu. Rev. Astron. Astrophys.* **23,** 119–146 (1985).
25. Harvey-Smith, L. *et al.* Faraday rotation of the supernova remnant G296.5+10.0: evidence for a magnetized progenitor wind. *Astrophys. J.* **712,** 1157–1165 (2010).
26. Zhang, B. A. 'Cosmic comb' model of fast radio bursts. *Astrophys. J.* **836,** L32 (2017).
27. Masui, K. *et al.* Dense magnetized plasma associated with a fast radio burst. *Nature* **528,** 523–525 (2015).
28. Petroff, E. *et al.* A real-time fast radio burst: polarization detection and multiwavelength follow-up. *Mon. Not. R. Astron. Soc.* **447,** 246–255 (2015).
29. Cordes, J. M. *et al.* Lensing of fast radio bursts by plasma structures in host galaxies. *Astrophys. J.* **842,** 35 (2017).
30. Manchester, R. N., Hobbs, G. B., Teoh, A. & Hobbs, M. The Australia telescope national facility pulsar catalogue. *Astron. J.* **129,** 1993–2006 (2005).

Acknowledgements We thank the staff of the Arecibo Observatory and the Green Bank Observatory for their help with our observations. We also thank B. Adebahr, L. Connor, G. Desvignes, R. Eatough, R. Fender, M. Haverkorn, A. Karastergiou, R. Morganti, E. Petroff, F. Vieyro and J. Weisberg for suggestions and comments on the manuscript. The Arecibo Observatory is operated by SRI International under a cooperative agreement with the National Science Foundation (AST-1100968), and in alliance with Ana G. Méndez-Universidad Metropolitana and the Universities Space Research Association. The Green Bank Observatory is a facility of the National Science Foundation operated under cooperative agreement by Associated Universities, Inc. Breakthrough Listen (BL) is managed by the Breakthrough Initiatives, sponsored by the Breakthrough Prize Foundation (http://www.breakthroughinitiatives.org). The research leading to these results received funding from the European Research Council (ERC) under the European Union's Seventh Framework Programme (FP7/2007-2013). J.W.T.H. is a Netherlands Organisation for Scientific Research (NWO) Vidi Fellow and, together with D.M., K.G. and C.G.B., acknowledges funding for this work from ERC Starting Grant DRAGNET under contract number 337062. L.G.S. acknowledges financial support from the ERC Starting Grant BEACON under contract number 279702, as well as the Max Planck Society. A.M.A. is an NWO Veni Fellow. S.C., J.M.C., P.D., T.J.W.L., M.A.M. and S.M.R. are partially supported by the NANOGrav Physics Frontiers Center (NSF award 1430284). V.M.K. holds the Lorne Trottier Chair in Astrophysics & Cosmology and a Canada Research Chair and receives support from an NSERC Discovery Grant and Herzberg Prize, from an R. Howard Webster Foundation Fellowship from the Canadian Institute for Advanced Research (CIFAR), and from the FRQNT Centre de Recherche en Astrophysique du Québec. C.J.L. acknowledges support from NSF award 1611606. Part of this research was carried out at the Jet Propulsion Laboratory, California Institute of Technology, under a contract with the National Aeronautics and Space Administration. B.M. acknowledges support from the Spanish Ministerio de Economía y Competitividad (MINECO) under grants AYA2016-76012-C3-1-P and MDM-2014-0369 of ICCUB (Unidad de Excelencia 'María de Maeztu'). S.M.R. is a CIFAR Senior Fellow. P.S. holds a Covington Fellowship at DRAO.

Author Contributions A.S. led the development of the Arecibo observing functionality used here and discovered the first bursts near 4.5 GHz. L.G.S. is Principal Investigator of the Arecibo monitoring campaign. D.M. discovered the rotation measure and analysed the burst properties in detail. K.G. searched all Arecibo datasets near 4.5 GHz for bursts. J.W.T.H. led the discussion on the interpretation of the results and writing of the manuscript. A.M.A. guided the development of the rotation measure fitting code. G.H.H. and C.S. performed the rotation measure synthesis and deconvolution analysis. G.C.B., S.C., J.M.C., V.G., V.M.K., C.J.L., M.A.M. and D.M. also contributed to the writing of the manuscript and analysis. V.G. observed, searched and detected bursts from the GBT at 6.5 GHz as a part of the BL monitoring campaign of known fast radio bursts. A.P.V.S. is the Principal Investigator of the BL project. C.B. helped with the polarization calibration of the test pulsar. G.H. wrote a code to splice raw voltages across computer nodes. All other co-authors contributed to the interpretation of the analysis results and to the final version of the manuscript.

Author Information Reprints and permissions information is available at www.nature.com/reprints. The authors declare no competing financial interests. Readers are welcome to comment on the online version of the paper. Publisher's note: Springer Nature remains neutral with regard to jurisdictional claims in published maps and institutional affiliations. Correspondence and requests for materials should be addressed to J.W.T.H. (J.W.T.Hessels@uva.nl).

Reviewer Information *Nature* thanks H. Falcke and the other anonymous reviewer(s) for their contribution to the peer review of this work.

METHODS

The analyses described here were based on the PRESTO[31], PSRCHIVE[32] and DSPSR[33] pulsar software suites, as well as custom-written Python scripts for linking utilities into reduction pipelines, fitting the data and plotting.

Observations and burst search. *Arecibo.* We made the observations using the Arecibo 'C-band' receiver (dual linear receptors) in the frequency range 4.1–4.9 GHz and the Puerto-Rican Ultimate Pulsar Processing Instrument (PUPPI) backend recorder. The full list of observations is reported in Extended Data Table 1. We operated PUPPI in its 'coherent search' mode, which produced 10.24 μs samples and 512 × 1.56 MHz frequency channels, each coherently dedispersed to dispersion measure 557.0 pc cm^{-3}. Coherent dedispersion within each 1.56-MHz channel means that the intra-channel dispersive smearing is smaller than 2 μs even if the dispersion measure of the burst is 10 pc cm^{-3} higher or lower than the fiducial value of 557.0 pc cm^{-3} used in the PUPPI recording. The raw PUPPI data also provide auto- and cross-correlations of the two linear polarizations, which can be converted to the Stokes parameters *I*, *Q*, *U* and *V* during post-processing. Before each observation, we performed a test scan on a known pulsar (PSR B0525+21) and a noise diode calibration scan (for polarimetric calibration).

Dedispersed time series with dispersion measure from 461 pc cm^{-3} to 661 pc cm^{-3} were searched using trial steps of 1 pc cm^{-3} and the PRESTO routine *single_pulse_search.py*, which applies a matched-filter technique to look for bursts with durations between 81.92 μs and 24,576 μs (for any putative burst that only has a single peak with width below 81.92 μs, the sensitivity will be degraded by a factor of a few at most). The resulting data points (dispersion measure, time, signal-to-noise ratio) were grouped into plausible astrophysical burst candidates using a custom sifting algorithm and then a dynamic spectrum of each candidate was plotted for manual inspection and grading. We found 16 bursts of astrophysical origin and used the DSPSR package to form full-resolution, full-polarization PSRCHIVE 'archive' format files for each burst.

Green Bank Telescope. On 26 August 2017, we observed FRB 121102 using the GBT 'C-band' receiver (4–8 GHz, with dual linear receptors) as part of a programme of monitoring known FRB positions. Observations were conducted with the Breakthrough Listen Digital Backend[34], which allowed recording of baseband voltage data across the entire nominal 4-GHz bandwidth of the selected receiver. Scans of a noise diode calibration, of the flux calibrator 3C161 and of the bright pulsar PSR B0329+54 supplemented the observations.

In post-processing, a total-intensity, low-resolution filterbank data product was searched for bursts with dispersion measure in the range 500–600 pc cm^{-3} using trial dispersion measure values in steps of 0.1 pc cm^{-3} and a search package implemented on an accelerated graphics processing unit to perform incoherent dedispersion[35]. We detected[36] 15 bursts with signal-to-noise ratio higher than 10. Here we present the properties of just the two brightest GBT bursts in order to confirm the large rotation measure observed by Arecibo and to quantify its variation in time. A detailed analysis of all GBT detections is in progress (V.G. *et al.*, manuscript in preparation). A section of raw voltage data (1.5 s) around each detected burst was extracted and coherently dedispersed to a nominal dispersion measure of 557.91 pc cm^{-3} using the DSPSR package. The final PSRFITS format data products have time and spectral resolutions of 10.24 μs and 183 kHz, respectively.

Data analysis. *Calculation of burst rotation measures.* We calibrated the burst 'archives' using the PSRCHIVE utility *pac* in 'SingleAxis' mode. This calibration strategy uses observations of a locally generated calibration signal (pulsed noise diode) to correct the relative gain and phase difference between the two polarization channels, under the assumption that the noise source emits equal power and has zero intrinsic phase difference in the two polarization channels. This calibration scheme does not correct for cross-coupling or leakage between the polarizations. While leakage must be present at some level, the high polarization fraction, complete lack of circular polarization, and consistency of the test pulsar observations with previous work give us confidence that calibration issues are not a substantial source of error for the rotation measure determination. In addition, the flux density of GBT observations was calibrated using the flux calibrator.

We initially performed a brute-force search for peaks in the linear polarization fraction (Extended Data Fig. 3) and discovered that $\mathrm{RM_{obs}} \approx +10^5$ rad m^{-2} in the Arecibo data. Each burst was corrected for Faraday rotation using the best-fit rotation measure value for that burst. Residual variations in the resulting polarization angle PA(λ) were used to refine the initial values by fitting

$$\mathrm{PA}(\lambda) = \mathrm{RM}\lambda^2 + \mathrm{PA}_\infty \quad (1)$$

and then

$$\hat{\boldsymbol{L}} = \exp[i2(\mathrm{RM}\lambda^2 + \mathrm{PA}_\infty)] \quad (2)$$

where $\hat{\boldsymbol{L}}$ is the unit vector of the linear polarization. We used equation (2) to fit the whole sample of bursts, imposing a different rotation measure per day and a different PA_∞ per telescope. The results of these fits are reported in Table 1 and an example is shown in Fig. 2.

By applying the optimal rotation measure value to each burst, we produced polarimetric profiles showing that each burst is almost 100% linearly polarized, after accounting for the finite widths of the PUPPI frequency channels (Fig. 1; Extended Data Fig. 2). In fact, the measured Arecibo bursts are depolarized to about 98%, in agreement with an uncorrected intra-channel Faraday rotation of

$$\Delta\theta = \frac{\mathrm{RM_{obs}} c^2 \Delta\nu}{\nu_c^3} \quad (3)$$

where *c* is the speed of light, $\Delta\nu$ is the channel width and ν_c is the central channel observing frequency. At 4.5 GHz, this corresponds to about 9°, and the depolarization fraction is

$$f_{\mathrm{depol}} = 1 - \frac{\sin(2\Delta\theta)}{2\Delta\theta} = 1.6\% \quad (4)$$

We supplemented the above analysis with a combination of the RM Synthesis method and the deconvolution procedure RMCLEAN (for example, Extended Data Fig. 4). Ensuring the presence of minimal Faraday complexity is possible by integrating across the full bandwidth and taking advantage of a Fourier transform relation between the observed $\boldsymbol{L}(\lambda^2)$ values and the Faraday spectrum (the polarized brightness as a function of rotation measure). This approach is known as RM Synthesis[37] and can be coupled with RMCLEAN to estimate the intrinsic Faraday spectrum[38]. Although RM Synthesis and RMCLEAN can have difficulty in properly reconstructing the intrinsic Faraday spectrum under certain circumstances, the spread of clean components is a reliable indicator of spectra that contain more than a single Faraday-unresolved source[39].

At each observed frequency, we integrated the Stokes parameters *Q* and *U* across the pulse width and normalized using the Stokes I profile. Owing to the normalization, we used only frequency bins that had a Stokes I signal-to-noise ratio of at least 5. We computed a deconvolved Faraday spectrum for each burst separately on a highly oversampled rotation measure axis (RM sampling $\delta\mathrm{RM} \approx 10^{-4}$ of the nominal full-width at half-maximum of the rotation measure resolution element). We used a relatively small gain parameter (0.02) and terminated the deconvolution when the peak of the residual decreased to 2σ above the mean. The algorithm typically required 50–80 iterations to converge. This combination of settings permits us to carefully consider the cumulative distribution of RMCLEAN components along the rotation measure axis and thus constrain the intrinsic width of the polarized emission to below about 0.1% of the typical rotation measure uncertainty. We found that this value scales with δRM because the peak of the Faraday spectrum rarely lands precisely on an individual pixel. To a high degree of confidence, there is evidence neither of emission at more than one rotation measure value, nor of a broadened ('Faraday-thick') emitting region; we therefore forgo more complicated fitting of the *Q* and *U* parameters[19]. The results of this analysis, shown in Extended Data Table 2, are consistent with the simplified fitting results described above.

Calculation of burst properties. As in previous studies[5,15], a search for periodicity in the burst arrival times remains inconclusive. Determining the exact dispersion measures of the bursts is complicated by their changing morphology with radio frequency[5,15]. Measuring the dispersion measure based on maximizing the peak signal-to-noise ratio of the burst often leads to blurring of the burst structure and, in the case of FRB 121102, an overestimation of the dispersion measure. We have thus chosen to display all bursts dedispersed to the same nominal dispersion measure of burst 6 (Fig. 1 and Extended Data Fig. 1). Taking advantage of the narrowness of burst 6, we estimated its optimal dispersion measure by minimizing its width at different dispersion measure trials. We measured burst widths at half the maximum of the peak value by fitting them with von Mises functions using the PSRCHIVE routine *paas* (Table 1). These widths correspond to the burst envelope in the case of multi-component bursts.

The flux densities of the Arecibo bursts were estimated using the radiometer equation to calculate the equivalent root-mean-square flux density of the noise

$$\sigma_{\mathrm{noise}} = \frac{T_{\mathrm{sys}}}{G\sqrt{2Bt_{\mathrm{int}}}} \quad (5)$$

where $T_{\mathrm{sys}} \approx 30$ K and $G \approx 7$ K Jy^{-1} are the system temperature and gain of the receiver, respectively, $B = 800$ MHz is the observing bandwidth and $t_{\mathrm{int}} = 10.24$ μs is the sampling time. The GBT observations were calibrated using a flux calibrator, as discussed earlier. Because of the complicated spectra of the bursts, we quote average values across the frequency band (Table 1).

The dynamic spectra of the bursts in Extended Data Fig. 1 show narrow-band striations that are consistent with diffractive interstellar scintillations caused by turbulent plasma in the Milky Way. The autocorrelation functions of the burst spectra show three features: a very narrow feature from radiometer noise, a narrow but resolved feature corresponding to the striations, and a broad feature related to the extent of the burst across the frequency band. The striation feature has a half-width that varies between about 2 MHz and 5 MHz from burst to burst and is comparable to the scintillation bandwidth expected from the Milky Way in the direction of FRB 121102. The NE2001 electron density model[40] provides an estimate $\tau \approx 16\,\mu s$ for the pulse broadening time at 1 GHz. This predicts a scintillation bandwidth of about $\nu^{4.4}/(2\pi\tau)$ that ranges from 5 MHz to 11 MHz across the 4.1–4.9 GHz band. We conclude that the measured autocorrelation functions and the NE2001 model prediction are consistent to within their uncertainties and that the narrow striations are due to Galactic scintillations.

A model for the rotation measure and scattering measure of FRB 121102. *Rotation measure constraints.* The measured $\mathrm{RM_{obs}} \approx +1 \times 10^5$ rad m^{-2} implies a source frame value

$$\mathrm{RM_{src}} = (1+z)^2 \mathrm{RM_{obs}} \approx +1.4 \times 10^5 \text{ rad m}^{-2} \quad (6)$$

We can use the previously estimated[8] $\mathrm{DM_{host}} \approx 70$–$270$ pc cm^{-3} (in the source frame) and $\mathrm{RM_{src}}$ to constrain the properties of the region in which the Faraday rotation occurs. In the absence of other information, we can set a constraint on the average magnetic field along the line of sight in the Faraday region using the ratio

$$B_\parallel = \frac{\mathrm{RM_{src}}}{0.81 \mathrm{DM_{host}}} = [0.6 \text{ mG}, 2.4 \text{ mG}] \quad (7)$$

If only a small portion of the total dispersion measure of FRB 121102 is from the highly magnetized region, the field could be much higher.

Scattering measure constraints. The best constraint on pulse broadening comes from the measurement of the scintillation (diffraction) bandwidth of $\Delta\nu_\mathrm{d} \approx 5$ MHz at 4.5 GHz (see above). This implies a pulse broadening time at 1 GHz of

$$\tau(1 \text{ GHz}) \approx (2\pi\Delta\nu_\mathrm{d})^{-1} \times (4.5 \text{ GHz}/1 \text{ GHz})^{4.4} = 24\,\mu s \quad (8)$$

This scattering time is consistent with that expected from the Milky Way using the NE2001 model[40] and therefore is an upper bound on any contribution from the host galaxy. Compared to scattering in the Milky Way, this upper bound is below the mean trend for any of the plausible values of $\mathrm{DM_{host}}$, especially when the correction from spherical to plane waves is taken into account[41].

Compared with the observer frame, the ratio $\tau/\mathrm{DM_{host}}$ is a factor of $(1+z)^2 = 1.42$ larger in the source frame but that is still far from sufficient to account for the apparent scattering deficit with respect to the Galactic τ/DM ratio. Given the apparent extreme conditions of the plasma in the host galaxy, it would not be surprising if its turbulence properties caused a scattering deficit. For example, scattering is reduced if the inner scale is comparable to or larger than the Fresnel scale owing to either a large magnetic field or a high temperature.

Constraints on the properties of the Faraday region. Comparison of the magnetic field and thermal energy densities enables us to constrain the electron density and temperature and the length scale of the region responsible for the observed Faraday rotation. We parametrize this relation with

$$\beta \frac{B^2}{8\pi} = 2 n_\mathrm{e} k_\mathrm{B} T_\mathrm{e} \quad (9)$$

where β is a scaling factor, B is the magnetic field strength and k_B is the Boltzmann constant. This assumes a 100% ionized gas of pure hydrogen with temperature equilibration between protons and electrons. Under equipartition, $\beta = 1$. In more densely magnetized regions, $\beta \ll 1$. Field reversals will reduce the total rotation measure, requiring a lower value of β in order to match constraints. The absence of free–free absorption at a frequency of about 1 GHz sets an additional constraint on the permitted parameter space.

In Extended Data Fig. 6, we explore a range of physical environments. We consider a lower limit, $\mathrm{DM} = 1$ pc cm^{-3}, on the dispersion measure that is smaller than the previously estimated[8] $\mathrm{DM_{host}} \approx 70$–$270$ pc cm^{-3} because it is possible that not all of the dispersion measure originates from the Faraday region. Galactic H II regions typically have $|\mathrm{RM}|$ smaller than about 3×10^2 rad m^{-2} and weak magnetic fields[42] with β greater than about 1, although calculations suggest that it is possible for H II regions to achieve high rotation measures under some circumstances[43]. The parameter space for a typical H II-region plasma at $T_\mathrm{e} = 10^4$ K is almost entirely excluded, and many possible H II region sizes and densities[21] are incompatible with the $\mathrm{DM_{host}}$ constraints. At higher T_e, wide ranges of the parameter space are permitted. In the case of equipartition, we have explicit unique solutions. For $T_\mathrm{e} = 10^6$ K, we find a density of $n_\mathrm{e} \approx 10^2$ cm^{-3} on a length scale $L_\mathrm{RM} \approx 1$ pc, comparable to the upper limit of the size of the persistent source. Higher-temperature gas ($T_\mathrm{e} = 10^8$ K) can be extended to $L_\mathrm{RM} \approx 100$ pc. For both of these solutions, the characteristic magnetic field strength is about 1 mG.

The large rotation measure of FRB 121102 is similar to those seen towards massive black holes; notably, $\mathrm{RM} \approx -5 \times 10^5$ rad m^{-2} is measured near Sagittarius A*, the Milky Way's central black hole, and probes scales below 10^4 Schwarzschild radii (about 0.001 pc)[11,12]. The constraints on n_e, T_e and L_RM are also consistent with the environment around Sagittarius A* (Extended Data Fig. 6). The high rotation measure towards the Galactic Centre magnetar PSR J1745−2900 (Fig. 3), $\mathrm{RM} = -7 \times 10^4$ rad m^{-2}, at a projected distance[23,44] of about 0.1 pc from Sagittarius A*, is evidence of a dynamically organized magnetic field around Sagittarius A* that extends to the distance of the magnetar[23]. Notably, radio monitoring of PSR J1745−2900 for about 4.5 years has shown a decrease of around 5% in the magnitude of the observed rotation measure, while the dispersion measure remained constant at a level of about 1% (Desvignes, G. *et al.*, manuscript in preparation). This suggests large fluctuations in magnetic field strength in the Galactic Centre on scales of roughly 10^{-5} pc.

The high rotation measure and the rich variety of other phenomena[4,5,7–10,15,16] displayed by the FRB 121102 system suggest that the persistent radio counterpart to FRB 121102 could represent emission from an accreting massive black hole, with the surrounding star formation representing a circum-black-hole starburst. Given the mass of the host galaxy and typical scaling relationships[45], the mass of the black hole would be about 10^4–10^6 solar masses ($M_\odot$). The observed radio brightness and compactness of the source, as well as the optical and X-ray non-detections[8,10,16], are compatible with such a black hole and an inefficient accretion state (about $10^{-6} L_\mathrm{Edd}$–$10^{-4} L_\mathrm{Edd}$, where L_Edd is the Eddington luminosity).

While models considering the presence of only a massive black hole have been proposed[46], there is no observational precedent for microsecond bursts created in such environments. Rather, the FRB 121102 bursts themselves could arise from a neutron star, perhaps highly magnetized and rapidly spinning, near an accreting massive black hole. The proximity of PSR J1745−2900 to Sagittarius A* demonstrates that such a combination is possible. In this model, the black hole is responsible for the observed persistent source, whereas the bursts are created in the magnetosphere of the nearby neutron star[47].

Alternatively, the association of FRB 121102 with a persistent radio source has been used to argue that the radio bursts are produced by a young magnetar powering a luminous wind nebula[13,48]. This model is not well motivated by Galactic examples, since the most luminous (non-magnetar-powered) Galactic pulsar wind nebula is 500,000 times less luminous than the persistent source that is coincident with FRB 121102, and Galactic magnetars have no detectable persistent radio wind nebulae[49,50]. Also, although giant flares from magnetars can produce relativistic outflows[51], an upper limit of the rotation measure from one such outburst[52] is four orders of magnitude below that observed for FRB 121102.

Nonetheless, under the millisecond magnetar model, the properties of the persistent source constrain the age of the putative magnetar to between several years and several decades, with a spin-down luminosity of 10^8 to 10^{12} times higher than any local analogue[13]. Furthermore, the millisecond magnetar model predicts that the nebula magnetic field strength scales with the integrated spin-down luminosity of the magnetar[13,48]. Extended Data Fig. 6 shows a range of sizes, densities and temperatures for the Faraday-rotating medium that are consistent with Crab-like pulsar wind nebulae, known supernova remnants and a simple model for swept-up supernova ejecta.

Data availability. The calibrated burst data are available upon request from the corresponding author.

Code availability. The codes used to analyse the data are available at the following sites: PRESTO (https://github.com/scottransom/presto), PSRCHIVE (http://psrchive.sourceforge.net) and DSPSR (http://dspsr.sourceforge.net).

31. Ransom, S. M. *New Search Techniques for Binary Pulsars.* PhD thesis, Harvard Univ. (2001); http://adsabs.harvard.edu/abs/2001PhDT.....123R.
32. van Straten, W., Demorest, P. & Oslowski, S. Pulsar data analysis with PSRCHIVE. *Astron. Res. Technol.* **9,** 237–256 (2012).
33. van Straten, W. & Bailes, M. DSPSR: digital signal processing software for pulsar astronomy. *Publ. Astron. Soc. Aust.* **28,** 1–14 (2011).
34. MacMahon, D. H. E. *et al.* The breakthrough listen search for intelligent life: a wideband data recorder system for the Robert C. Byrd green bank telescope. *Publ. Astron. Soc. Pac.* (in the press); preprint at https://arxiv.org/abs/1707.06024 (2017).
35. Barsdell, B. R., Bailes, M., Barnes, D. G. & Fluke, C. J. Accelerating incoherent dedispersion. *Mon. Not. R. Astron. Soc.* **422,** 379–392 (2012).
36. Gajjar, V. *et al.* FRB 121102: detection at 4–8 GHz band with Breakthrough Listen backend at Green Bank. *Astron. Telegr.* **10675** (2017).
37. Brentjens, M. A. & de Bruyn, A. G. Faraday rotation measure synthesis. *Astron. Astrophys.* **441,** 1217–1228 (2005).

38. Heald, G., Braun, R. & Edmonds, R. The Westerbork SINGS survey. II. Polarization, Faraday rotation, and magnetic fields. *Astron. Astrophys.* **503,** 409–435 (2009).
39. Anderson, C. S., Gaensler, B. M., Feain, I. J. & Franzen, T. M. O. Broadband radio polarimetry and Faraday rotation of 563 extragalactic radio sources. *Astrophys. J.* 815, 49 (2015); erratum 820, 144 (2016).
40. Cordes, J. M. & Lazio, T. J. W. NE2001.I. A new model for the galactic distribution of free electrons and its fluctuations. Preprint at http://arxiv.org/abs/astro-ph/0207156 (2002).
41. Cordes, J. M., Wharton, R. S., Spitler, L. G., Chatterjee, S. & Wasserman, I. Radio wave propagation and the provenance of fast radio bursts. Preprint at https://arxiv.org/abs/1605.05890 (2016).
42. Harvey-Smith, L., Madsen, G. J. & Gaensler, B. M. Magnetic fields in large-diameter H II regions revealed by the Faraday rotation of compact extragalactic radio sources. *Astrophys. J.* **736,** 83 (2011).
43. Sicheneder, E. & Dexter, J. A single H II region model of the strong interstellar scattering towards Sgr A*. *Mon. Not. R. Astron. Soc.* **467,** 3642–3647 (2017).
44. Shannon, R. M. & Johnston, S. Radio properties of the magnetar near Sagittarius A* from observations with the Australia Telescope Compact Array. *Mon. Not. R. Astron. Soc.* **435,** L29–L32 (2013).
45. Reines, A. E. & Volonteri, M. Relations between central black hole mass and total galaxy stellar mass in the local universe. *Astrophys. J.* **813,** 82 (2015).
46. Vieyro, F. L., Romero, G. E., Bosch-Ramon, V., Marcote, B. & del Valle, M. V. A model for the repeating FRB 121102 in the AGN scenario. *Astron. Astrophys.* **602,** A64 (2017).
47. Pen, U.-L. & Connor, L. Local circumnuclear magnetar solution to extragalactic fast radio bursts. *Astrophys. J.* **807,** 179 (2015).
48. Kashiyama, K. & Murase, K. Testing the young neutron star scenario with persistent radio emission associated with FRB 121102. *Astrophys. J.* **839,** L3 (2017).
49. Hester, J. J. The Crab Nebula: an astrophysical chimera. *Annu. Rev. Astron. Astrophys.* **46,** 127–155 (2008).
50. Reynolds, S. P. *et al.* Pulsar-wind nebulae and magnetar outflows: observations at radio, x-ray, and gamma-ray wavelengths. *Space Sci. Rev.* **207,** 175–234 (2017).
51. Frail, D. A., Kulkarni, S. R. & Bloom, J. S. An outburst of relativistic particles from the soft γ-ray repeater SGR1900+14. *Nature* **398,** 127–129 (1999).
52. Gaensler, B. M. *et al.* An expanding radio nebula produced by a giant flare from the magnetar SGR 1806-20. *Nature* **434,** 1104–1106 (2005).
53. McKee, C. F. & Truelove, J. K. Explosions in the interstellar medium. *Phys. Rep.* **256,** 157–172 (1995).
54. Orlando, S., Miceli, M., Pumo, M. L. & Bocchino, F. Modeling SNR Cassiopeia A from the supernova explosion to its current age: the role of post-explosion anisotropies of ejecta. *Astrophys. J.* **822,** 22 (2016).
55. McCray, R. & Fransson, C. The remnant of supernova 1987A. *Annu. Rev. Astron. Astrophys.* **54,** 19–52 (2016).

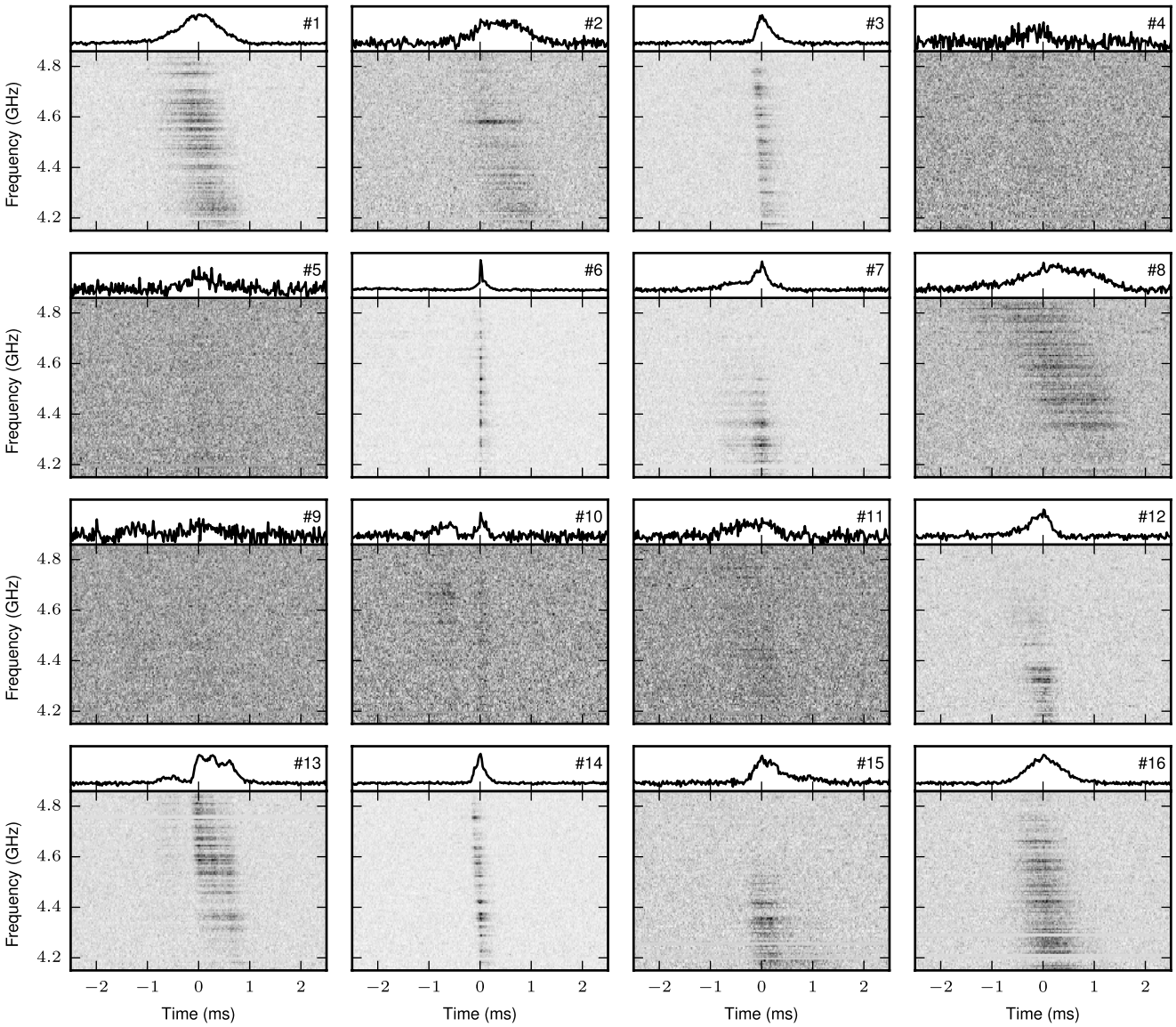

Extended Data Figure 1 | Pulse profiles and spectra of 16 Arecibo bursts. The bursts are dedispersed to DM = 559.7 pc cm^{-3} (which minimizes the width of burst 6) and plotted with time and frequency resolutions of 20.48 μs and 6.24 MHz, respectively.

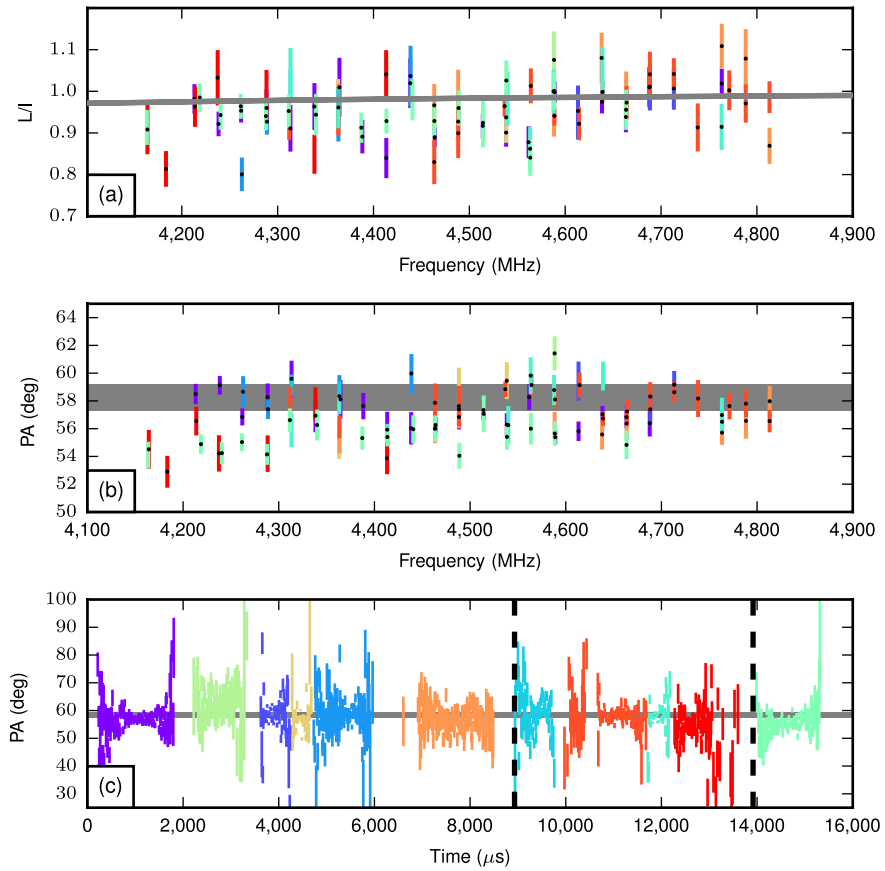

Extended Data Figure 2 | Polarimetric properties of the 11 brightest bursts detected by Arecibo. a, Linear polarization fraction of the bursts as a function of frequency. The solid line shows the theoretical depolarization due to intra-channel Faraday rotation, calculated using equations (3) and (4). **b**, PA_∞ as a function of frequency. Values in **a** and **b** are averaged over 16 consecutive channels. **c**, PA_∞ as a function of time. A time offset is applied to each burst in order to show them consecutively. Vertical dashed lines divide different observing sessions. All values in this figure have been corrected for the rotation measure, which was calculated with a global fit. Grey regions in **b** and **c** indicate the 1σ uncertainty around the polarization angle determined from the global fit.

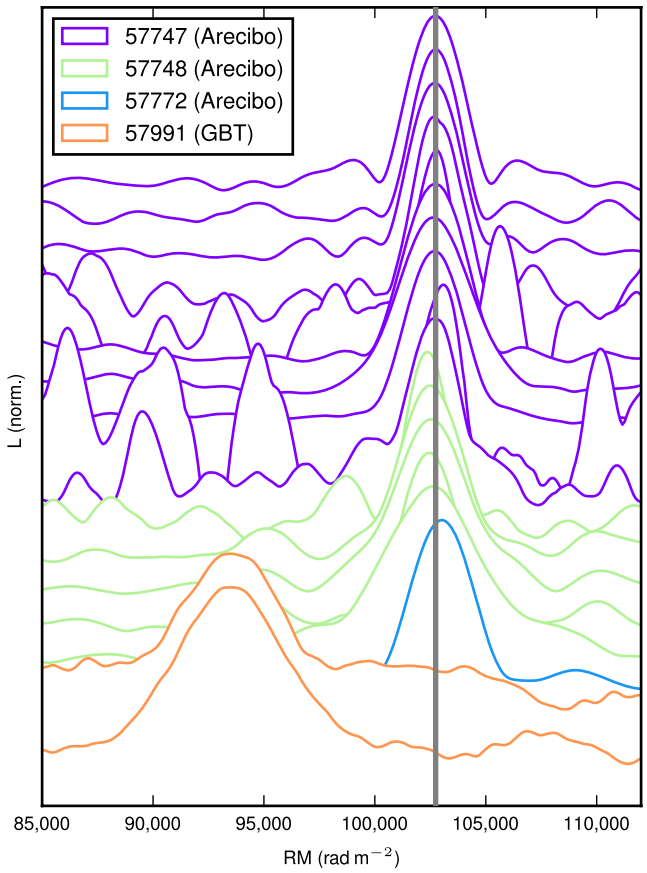

Extended Data Figure 3 | Linear polarization fraction of the bursts as a function of rotation measure. Different colours represent different observing sessions (see key). The grey line indicates the average rotation measure that yields the largest polarization fraction in the first observing session.

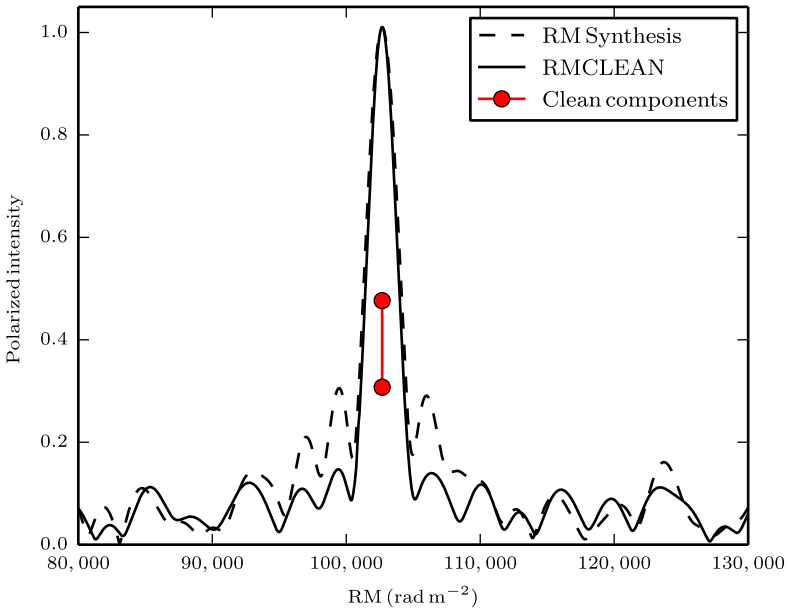

Extended Data Figure 4 | Example of RM Synthesis and RMCLEAN results for burst 8. The relevant rotation measure range is shown for burst 8, after analysis with RM Synthesis (dashed line) and RMCLEAN (solid line), as described in the main text. Only two clean components (red circles) were required to reach convergence in the deconvolution algorithm (at 102,679.5 rad m^{-2} and 102,679.75 rad m^{-2}; compare with the peak of the final deconvolved Faraday spectrum at 102,679.65 rad m^{-2}). For all bursts, the RM Synthesis and RMCLEAN steps demonstrate an extremely thin and single-peaked Faraday spectrum.

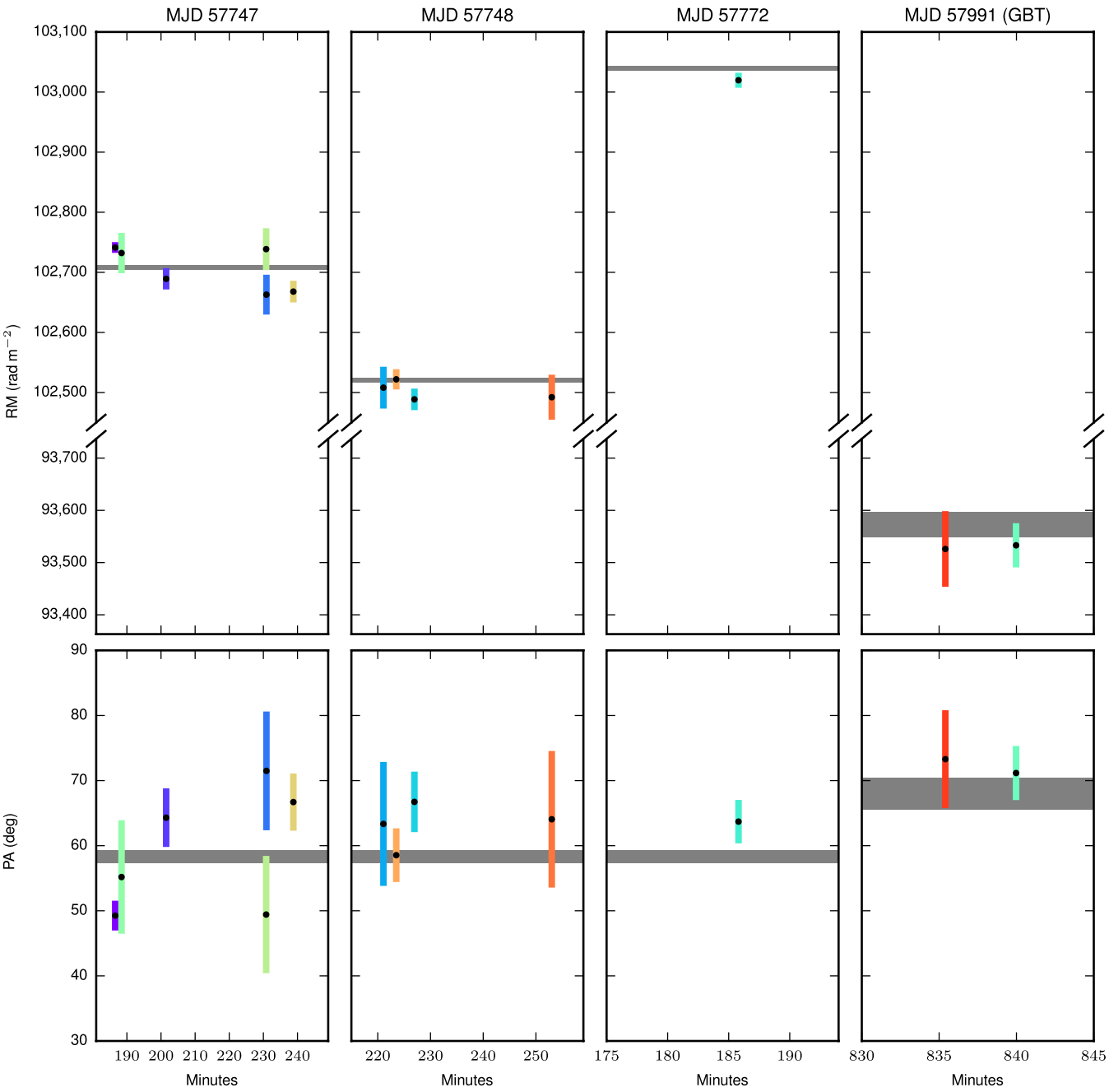

Extended Data Figure 5 | Rotation measure and PA_∞ values of different bursts. Coloured, 1σ error bars represent individual bursts, with central values highlighted by black dots. Horizontal grey regions are values obtained from a global fit. MJD, modified Julian date. Values used in the figure are reported in Table 1.

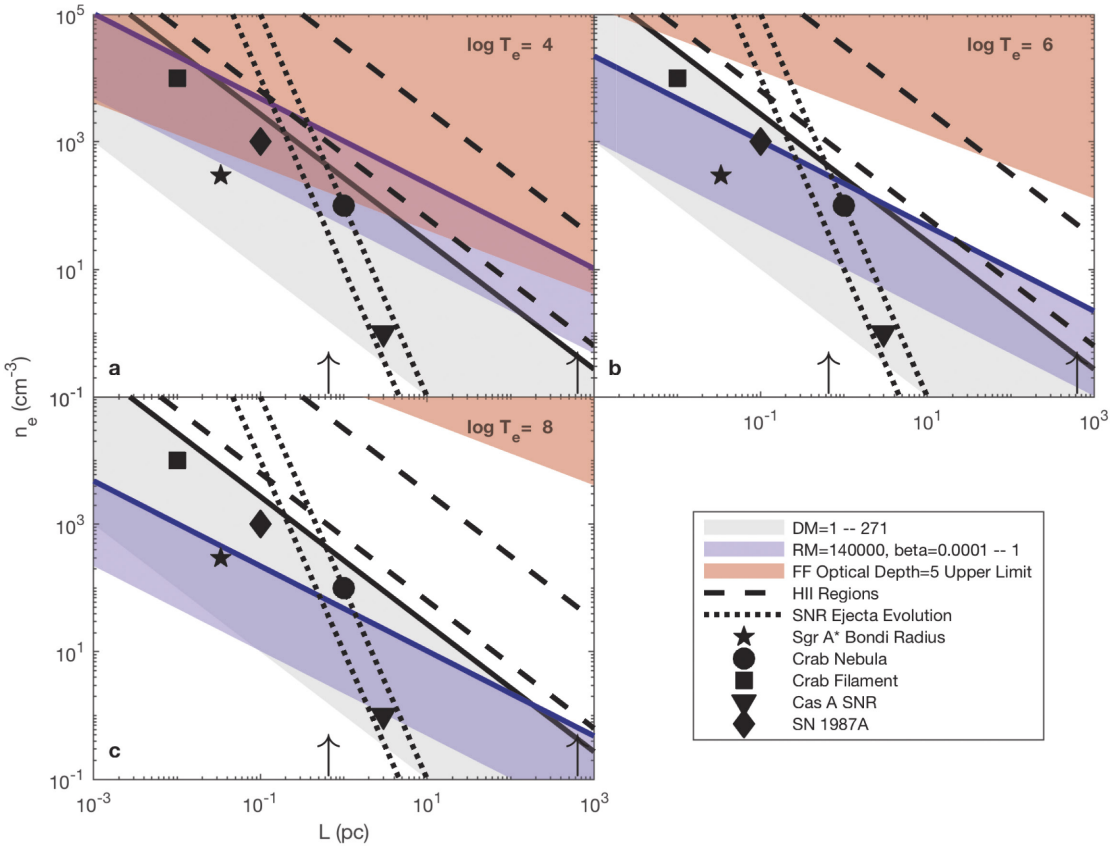

Extended Data Figure 6 | Physical constraints from source parameters. **a**–**c**, Parameter space for the electron density (n_e) and length scale (L_{RM}) of the Faraday region for three different temperature regimes, $T_e = 10^4$ K (**a**), 10^6 K (**b**) and 10^8 K (**c**). The shaded red region indicates the parameter space excluded because of optical depth considerations (optical depth from free–free absorption $\tau_{ff} > 5$). The solid black line indicates the maximum DM_{host} permitted, while the shaded grey region shows the dispersion measure down to 1 pc cm^{-3}. The solid blue line denotes RM_{src}. The shaded blue region shows the range $10^{-4} \leq \beta \leq 1$. The intersection of grey and blue regions outside of the red region is physically permitted. The arrows indicate the upper limits on the sizes of the persistent source (left) and the star-forming region (right), respectively[8,10]. The parallel dashed lines represent fits to a range of Galactic and extragalactic H II regions[21]. The parallel dotted lines represent the evolution of $1M_\odot$ and $10M_\odot$ of ejecta in up to 1,000 years at a velocity of 10^4 km s^{-1} in the blast-wave phase following a supernova[53]. The filled downward-pointing triangles and diamonds correspond to the supernova remnants Cas A and SN 1987A, respectively[54,55]. The filled circles represent the mean density and diameter of the Crab Nebula, whereas the filled squares represent the characteristic density and length scale of a dense filament in the Crab Nebula[24]. The stars indicate the density of Sagittarius A* at the Bondi radius[22].

Extended Data Table 1 | List of 4.5-GHz Arecibo observations used in this study

Start (MJD)	Duration (s)	# bursts
57717.2018171	4146	0
57717.2500000	2378	0
57747.1172685	6703	10
57748.1141435	6806	5
57772.0590625	5901	1
57806.9996759	2700	0
57813.9342940	5588	0
57821.9134144	2893	0
57858.8624769	2350	0
57865.8491782	1904	0
57872.8160417	2919	0
57900.7106597	2779	0

Extended Data Table 2 | Results of analysis with RM Synthesis and RMCLEAN

Burst	RM (rad m^{-2})	RM disp (rad m^{-2})
1	+102805 ± 37	< 0.12
2	+102685 ± 70	< 0.05
3	+102667 ± 37	< 0.12
6	+102642 ± 73	< 0.11
7	+102643 ± 105	< 0.04
8	+102680 ± 43	< 0.12
12	+102585 ± 67	< 0.02
13	+102484 ± 53	0
14	+102440 ± 51	0
15	+102701 ± 211	< 0.05
16	+102986 ± 27	< 0.10
GBT-1	+93572 ± 2885	0
GBT-2	+93523 ± 237	0

Rotation measures were determined by fitting a quadratic function to the peak of the deconvolved Faraday spectrum. Rotation measure uncertainties were determined by dividing the nominal full-width at half-maximum of the rotation measure resolution element by twice the signal-to-noise ratio at the peak of the rotation measure spectrum. RMdisp is the second moment (dispersion) of the RMCLEAN clean components discovered during the Faraday spectrum deconvolution. Upper limits indicate that the value scales with the rotation measure pixel size; a zero value means that all clean components fell within the same pixel and indicates a Faraday spectrum that is indistinguishable from being infinitely thin.